Complex changes in structural parameters hidden in the universal phase diagram of the quasi-one-dimensional organic conductors $(TMTTF)_2X$ ($X = NbF_6$, AsF_6, PF_6, and Br)

Shunsuke Kitou,[1,*] Lidong Zhang,[1] Toshikazu Nakamura,[2] and Hiroshi Sawa[1,†]
[1]*Department of Applied Physics, Nagoya University, Nagoya 464-8603, Japan*
[2]*Institute for Molecular Science, Myodaiji, Okazaki 444-8585, Japan*

(Received 18 March 2021; revised 3 May 2021; accepted 17 May 2021; published 27 May 2021)

Structural parameters in quasi-one-dimensional organic conductors $(TMTTF)_2X$ ($X = NbF_6$, AsF_6, PF_6, and Br) are investigated by synchrotron x-ray diffraction. The temperature dependences of the crystal structures differ significantly between octahedral and monatomic anion systems, corresponding to the presence or absence of a charge-ordering transition. Changes in temperature and chemical pressure control the dimensionality of the lattice and the degree of dimerization. Furthermore, the antiferromagnetic and spin-Peierls ground states in this system depend on the spin frustration due to transfer integral paths between the one-dimensional chain molecules.

DOI: 10.1103/PhysRevB.103.184112

I. INTRODUCTION

Even a molecular conductor with a simple molecular arrangement can be made to exhibit various electronic phases by controlling the temperature and pressure [1–7], because quantum parameters such as the transfer integral and the Coulomb interaction are antagonistic. These parameters can change in response to even slight alterations in molecular structure and arrangement. Approximate theoretical models have succeeded in partially explaining the physical properties of such systems [8–11]. However, to understand fully their various physical properties on the pressure-temperature (*P*-*T*) phase diagram, discussions based on precise crystal structures are indispensable.

Because of the simplicity of its molecular structures and their arrangement, the quasi-one-dimensional (1D) molecular conductor $(TMTTF)_2X$ [12], a $\frac{3}{4}$-filled system, is ideal for discussing the relationship between electronic correlations and crystal structure. Here, TMTTF is tetramethyltetrathiafulvalene, and X^- is a monovalent anion. The $(TMTTF)_2X$ salt, which consists of weak dimers of TMTTF molecules stacked in the *a*-axis direction, shows various electronic phases on the *P*-*T* phase diagram: metallic, dimer Mott insulator (DMI), charge ordering (CO), antiferromagnetic (AFM), spin Peierls (SP), spin density wave, and superconducting [12–59]. In particular, it is interesting (1) that the SP phase exists between the two different AFM phases as the ground state and (2) how the CO state affects the AFM and SP transitions [Fig. 1(b)]. Previous nuclear magnetic resonance (NMR) studies point out that the magnetic order patterns are different between the AFM-I and AFM-II states [37,38].

The physical and structural properties of this system have been investigated by transport [13–15], magnetic [16], dielectric [17–20], optical [21–23], resonance [24–40], and scattering [12,41–51] measurements, and many theoretical models have been proposed [60–67]. However, there is no unified understanding of the order parameters that govern its physical properties, because it is difficult to determine the precise structural parameters of a system with such low symmetry. In particular, although structural changes associated with the CO state have been confirmed by high-resolution thermal expansion measurements [54–56], the precise structural parameters in the CO phase have been unknown.

Our previous structural study elucidated the CO state of $(TMTTF)_2PF_6$ not only from the crystal structure but also from the valence electron density (VED) obtained by synchrotron x-ray diffraction (XRD) experiments [50]. In this study, we investigate the detailed structural changes of $(TMTTF)_2X$ when the temperature and the anion X are changed ($X = NbF_6$, AsF_6, PF_6, and Br). These salts have different magnetic ground states as shown in Fig. 1(b). We report a $(TMTTF)_2X$ salt ($X = NbF_6$); its CO and AFM transitions were observed by electron spin resonance (ESR) measurements. High-quality single crystals for precise structural analysis could not be obtained from the $X = SbF_6$ salt, the physical properties of which have been well investigated. Therefore, we used the $X = NbF_6$ salt to discuss this series of systems; the CO and AFM transition temperatures of $X = NbF_6$ are similar to those of $X = SbF_6$. Our precise structural investigations provide insights into the order parameters that govern the CO and magnetic order states in this system.

II. EXPERIMENTS

X-band continuous-wave ESR measurements for a $(TMTTF)_2NbF_6$ crystal were conducted using a Bruker E500 spectrometer with a ^{4}He flow cryostat (Oxford Cryostat E900). ESR measurements were performed on a single crystal

*Present address: RIKEN Center for Emergent Matter Science, Wako, Saitama 351-0198, Japan; shunsuke.kito@riken.jp
†hiroshi.sawa@cc.nagoya-u.ac.jp

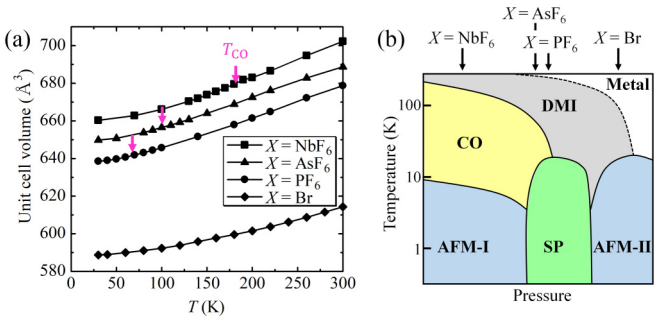

FIG. 1. (a) Temperature dependence of the unit cell volumes of $(TMTTF)_2X$. The charge-ordering transition temperatures of $X =$ NbF_6, AsF_6, and PF_6 are marked at $T_{CO} = 165$, 102 [30], and 65 K [31], respectively. (b) A schematic pressure-temperature phase diagram of $(TMTTF)_2X$, which is drawn with reference to [6,52].

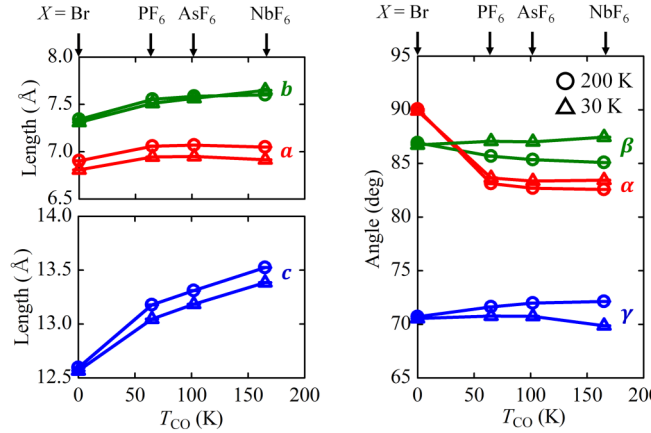

FIG. 2. Anion dependence of the lattice parameters of $(TMTTF)_2X$ at 200 and 30 K. The horizontal axis indicates the charge-ordering transition temperature. The values of $X =$ Br are temporally plotted at $T_{CO} = 0$ K.

that was set in a quartz rod using silicone grease. The temperature range was 8–297 K. The spectrum was recorded using the following parameters: microwave frequency: 9.674 GHz; microwave power: 4 mW; amplitude modulation: 0.01–0.05 mT. The XRD experiments using single crystals were performed on the BL02B1 beamline [68] at the synchrotron radiation facility SPring-8 in Japan. A helium gas blowing device was employed to cool the sample. A two-dimensional (2D) CdTe PILATUS was used as the detector. The incident energy of the synchrotron x rays was $E \cong 40$ keV. Diffraction intensity averaging and structural analysis were performed using SORTAV [69] and JANA2006 [70], respectively. To determine the structural parameters with high accuracy, the structural refinement was performed using only the high-angle intensity ($\sin\theta/\lambda \geqslant 0.5$ Å^{-1}) (i.e., high-angle analysis [50]). Here, λ is the wavelength of the incident x ray, and θ is the XRD angle. The transfer integrals of $(TMTTF)_2X$ were calculated by the extended Hückel method [71]. A core differential Fourier synthesis (CDFS) method [72] was used for the electron density analysis.

III. RESULTS AND DISCUSSIONS

First, we focus on $(TMTTF)_2Br$, in which the unit cell volume is considerably smaller than that of other salts with the octahedral counter anions [Fig. 1(a)]. The $X =$ Br salt shows a metal-insulator transition at 100 K and has a wider metal temperature range than other salts [13]. Previous high-resolution thermal expansion measurements detected a peak anomaly that may be associated with the metal-insulator transition [55]. On the other hand, in the temperature dependence of the unit cell volume [Fig. 1(a)], there is no obvious anomaly near the transition temperature. The temperature dependence of $X =$ Br show a monotonous decrease, which is similar to the other salts.

The lattice parameters of each salt, where the crystal system is triclinic, are summarized in Table S1 in the Supplemental Material [73]. The value of the α angle of $X =$ Br is significantly different from that of the other salts (∼10%) (Fig. 2); this has a strong influence on the values of transfer integrals between the TMTTF 1D chains, as described later. This difference in the α angle of $X =$ Br corresponds to the absence of steric hindrance of the octahedron.

Figure 3(a) shows the temperature dependence of the normalized lattice parameters of $X =$ Br. The a axis, which is the stacking direction of TMTTF molecules, becomes shorter as the temperature decreases, whereas the b and c axes and angles show almost no temperature dependence. These dependences can be interpreted as the behavior of the simple $\frac{3}{4}$-filled salt, which has a 1D stacking structure of dimerized TMTTF molecules.

Next, the $(TMTTF)_2X$ system with octahedral anions was investigated. Structural analysis reveals that the crystal structure of the recently synthesized salt $(TMTTF)_2NbF_6$ is the same as that of the other members of the $(TMTTF)_2X$ series [Fig. 4(a)]. We investigated the electronic states by ESR measurements. The temperature dependence of the ESR parameters for $(TMTTF)_2NbF_6$ is shown in Figs. 4(b)–4(d). Figure 4(b) shows the temperature dependence of the spin susceptibility χ_{spin} for a single crystal as an external static field is applied along the three orthogonal crystal axes. The g values are explained by the g tensor of the TMTTF radical and molecular orientation. The g values along the b' and c^* axes show slight temperature changes [Fig. 4(c)].

At around 165 K, the ESR linewidth $\Delta H_{p.p.}$ shows a hump [Fig. 4(d)], although no obvious change in χ_{spin} was observed [Fig. 4(b)]. Also, a hump is observed around 260 K in Fig. 4(b). However, the experimental accuracy is a little poor because the high-temperature part is affected by the skin effect. Furthermore, since the humplike behavior was not reproducible, we concluded the feature is an experimental error. Below 150 K, the anisotropy of $\Delta H_{p.p.}$ gradually changes to 40 K. While $\Delta H_{p.p.}$ ($\parallel a$) and $\Delta H_{p.p.}$ ($\parallel b'$) decrease as the temperature decreases, $\Delta H_{p.p.}$ ($\parallel c^*$) is almost temperature independent down to 40 K. (An abrupt increase of $\Delta H_{p.p.}$ below 30 K for all directions is considered to be a precursor phenomenon of the AFM phase transition.) The behavior of the ESR spectra is similar to that of $(TMTTF)_2SbF_6$ [28,36] and $(TMTTF)_2TaF_6$ [32].

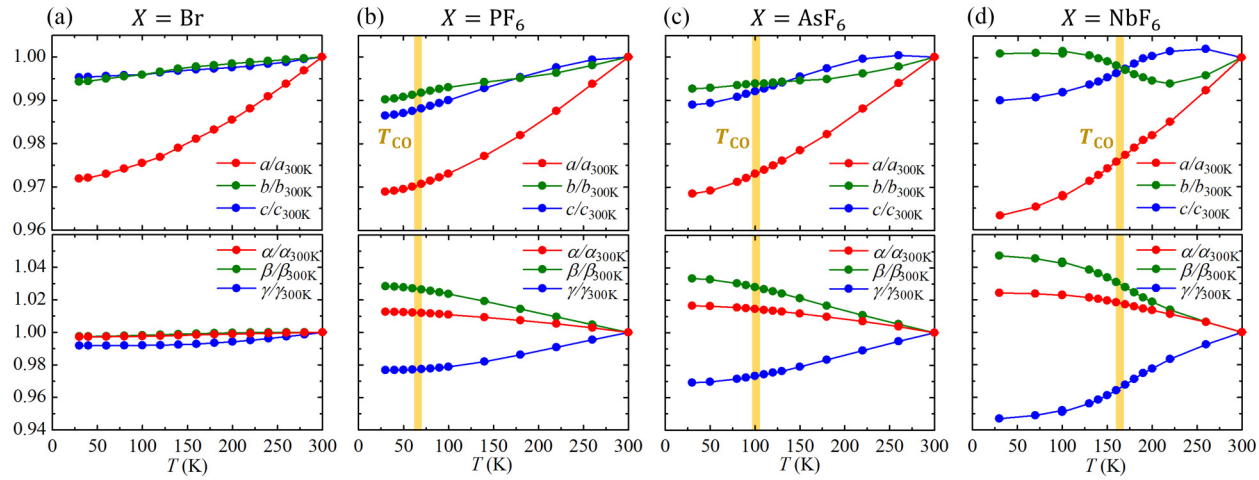

FIG. 3. Temperature dependence of the lattice parameters of $(TMTTF)_2X$. Each value is normalized with values at 300 K.

The CO and AFM transition temperatures of $(TMTTF)_2NbF_6$ are $T_{CO} = 165$ K and $T_{AFM} = 10$ K, respectively, which are about the same as the values for $(TMTTF)_2SbF_6$: $T_{CO} = 156$ K and $T_{AFM} = 8$ K [29]. Considering the change in the anion as a change in chemical pressure, this result is reasonable because the ionic radii of Nb^{5+} (0.64 Å) are slightly larger than those of Sb^{5+} (0.60 Å) [74].

In the $X = NbF_6$, AsF_6, and PF_6 salts, there is no clear anomaly corresponding to the metal-insulator and CO transitions in the temperature dependence of the unit cell volume [Fig. 1(a)]. On the other hand, the normalized lattice parameters show the characteristic temperature dependence [Figs. 3(b)–3(d)]. The a axis shows a temperature dependence similar to $X = Br$, whereas the b and c axes and angles differ greatly. These behaviors suggest that the structural effect of octahedral counter anions is important in the phase diagram of the $(TMTTF)_2X$ system showing the various electronic states.

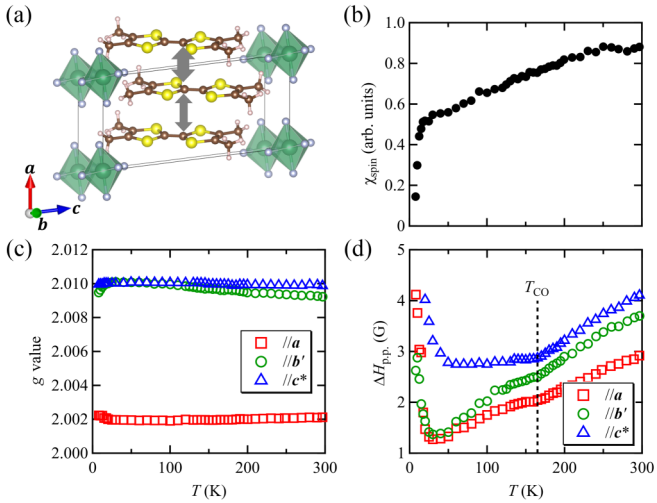

FIG. 4. (a) Crystal structure of $(TMTTF)_2NbF_6$. The temperature dependence of ESR parameters; (b) χ_{spin}, (c) g value, and (d) linewidth $\Delta H_{p.p.}$ for $(TMTTF)_2NbF_6$.

In fact, the importance of the interactions between donor and anion molecules is discussed in this system [49,57–59].

In addition, the rate of change of the lattice parameters (a axis and angles) with respect to temperature increases toward the low-pressure region, that is, from $X = PF_6$ to $X = NbF_6$ [Fig. 1(b)]. The T_{CO} is at the inflection point of the b axis, which is more noticeable at higher T_{CO}. In particular, the temperature dependence of the b axis in $X = NbF_6$ shows a negative thermal expansion. Because the b-axis direction corresponds to the interchain direction in the 2D TMTTF plane that causes the CO state [50], the characteristic temperature dependence may be related to the fluctuation toward the CO transition. In other words, the presence or absence of CO and its transition temperature greatly affect the anisotropy of the lattice with respect to temperature changes.

Next, we compared the crystal structure of each salt. Structural analysis confirmed the occurrence of structural changes corresponding to the CO state at 30 K for $X = NbF_6$, AsF_6, and PF_6. On the other hand, we could not confirm a clear tendency of the CO state, i.e., the breaking of the inversion symmetry, at 30 K for $X = Br$ from the structural analysis. However, previous dielectric constant, ESR, and NMR measurements have confirmed anomalies that may be associated with CO [17,28,39]. The reason why the clear CO was not observed at 30 K in $X = Br$ by the XRD experiment may be that the measured temperature is insufficient to detect CO and/or the amplitude of CO is quite small. The space group in the CO phase of $X = NbF_6$, AsF_6, and PF_6 is $P1$, and the same CO pattern indicating a 2D Wigner crystal state [50] was confirmed.

To investigate the change in the interactions between TMTTF molecules with respect to X and temperature, the transfer integrals t were evaluated. Each value is summarized in Table S9 in the Supplemental Material [73]. Figure 5(b) shows the transfer integrals at 200 K (DMI phase). The values of t_{a1} and t_{a2} in the stacking a-axis direction are approximately an order of magnitude larger than those in the interchain direction [$t_{b1}(= t_{b2})$ and t_{p1}], which suggests that this system is quasi-1D.

Figures 5(c) and 5(d) show the temperature dependence of the dimensionality t_A/t_B and the degree of dimerization

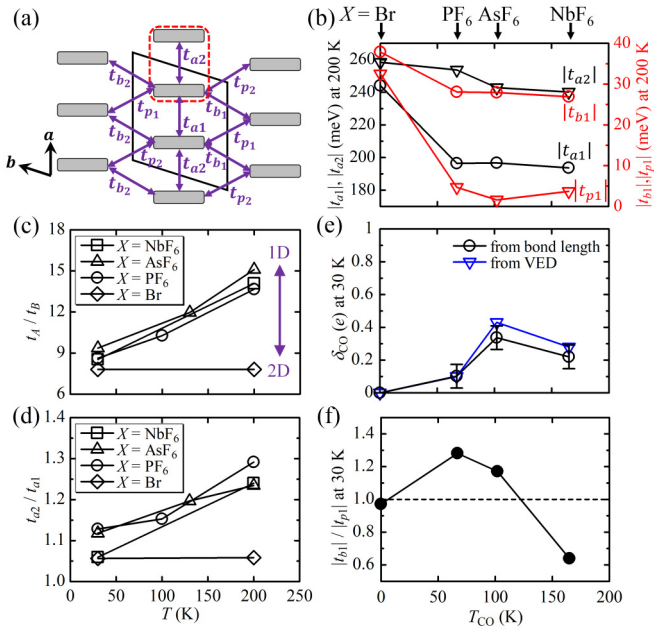

FIG. 5. (a) Definition of intermolecular transfer integrals t of $(TMTTF)_2X$. The black solid and red dotted lines indicate the unit cell and the TMTTF dimer, respectively. (b) Anion dependence of the transfer integrals at 200 K in the dimer Mott insulator phase. The horizontal axis indicates the charge-ordering transition temperature. Transfer integrals of X = Br are temporally plotted at $T_{CO} = 0$ K. Temperature dependence of (c) the dimensionality and (d) the degree of dimerization. Here, $t_A = (|t_{a1}| + |t_{a2}|)/2$ and $t_B = (|t_{b1}| + |t_{b2}| + |t_{p1}| + |t_{p2}|)/4$. (e) Anion dependence of the amplitude of charge-ordering δ_{CO} in the TMTTF dimer at 30 K. (f) Spin frustration factor $|t_{b1}|/|t_{p1}|$ between the one-dimensional chain molecules at 30 K.

of t_{a2}/t_{a1}, respectively. Here, $t_A = (|t_{a1}| + |t_{a2}|)/2$ and $t_B = (|t_{b1}| + |t_{b2}| + |t_{p1}| + |t_{p2}|)/4$. The X = Br salt has almost no temperature dependence on t_A/t_B and t_{a2}/t_{a1}. On the other hand, in salts with octahedral anions, these parameters show large changes with temperature. As the temperature decreases, t_A/t_B becomes smaller (i.e., the interchain interactions become more pronounced). In fact, because the charge-rich and charge-poor TMTTF molecules are so arranged by the intersite Coulomb interaction V to avoid each other in the CO phase [50], it is reasonable that two-dimensionality would increase at low temperature (LT).

There is a clear correlation between t_{a2}/t_{a1} and t_A/t_B [Figs. 5(c) and 5(d)]: the weaker the dimerization, the stronger the two-dimensionality. When the dimerization is weakened in the salts with octahedral anions, the V between molecules becomes more effective. As a result, the CO state stabilizes and the two-dimensionality increases in LT. This result corresponds to previous XRD studies [47] and theoretical calculations [66]. On the other hand, the X = Br salt is more conductive [13] and has larger transfer integrals [Fig. 5(b)] than other salts with octahedral anions. As a result, because the effect of V is weaker due to the Thomas-Fermi shielding, the CO transition temperature of X = Br may be lower and/or the amplitude of CO may be smaller than other salts with octahedral anions.

The amplitude of CO δ_{CO} in the TMTTF dimer was estimated from the bond length in the TMTTF molecule. A formula, $q = -15.55 + 20.42r$, is given for empirically calculating the valence of a TMTTF molecule in Ref. [75]. Here, q is the valence of the TMTTF, and $r(= a/b)$ is a ratio of the central (a) C = C bond and (b) C–S bonds length. The amount of charge transfer δ_{CO} in the TMTTF dimer is calculated as $\delta_{CO} = (q_{\text{hole–poor}} - q_{\text{hole–rich}})/2$. Figure 5(e) shows the anion dependence of δ_{CO} calculated from the bond length. We also estimated δ_{CO} by electron density analysis using the CDFS method. Almost no differences were observed in the appearance of the VED distributions of TMTTF molecules in X = NbF_6, AsF_6, PF_6, and Br (Fig. S2 in the Supplemental Material [73]) because the amount of charge transfer ($\delta_{CO} \leqslant 0.5e$) was too small compared to the number of valence electrons in a TMTTF molecule. By considering the number of valence electrons in the atomic basin of the respective atoms in the TMTTF molecule calculated by Bader's topological analysis [76], δ_{CO} was determined from the VED, producing almost the same numbers as the estimation from the bond length [Fig. 5(e)].

The δ_{CO} of X = AsF_6 is larger than that of X = PF_6 [77], which is consistent with the estimation from infrared [22], Raman [23], and NMR [27,30,31] spectroscopy. However, the δ_{CO} of X = NbF_6 is smaller than that of X = AsF_6, although the T_{CO} is higher. Assuming that the amplitude of T_{CO} in X = NbF_6 has about the same values as X = SbF_6, this tendency is not consistent with the results of infrared measurements [22]. However, the decrease in δ_{CO} toward the AFM phase transition temperature is observed in X = SbF_6 from NMR measurements [29,34]. Therefore, this tendency in X = NbF_6 may be related to the AFM fluctuations.

Finally, we discuss the magnetic ground state, which generally depends on the anisotropy and magnitude of the transfer integrals. If $(TMTTF)_2X$ were simply a 1D system, it would be impossible to explain why there are two different AFM phases on both sides of the SP phase [Fig. 1(b)]. However, since the four $(TMTTF)_2X$ salts are more 2D in the LT phase [Fig. 5(c)], carefully investigating the interactions between the 1D-chain molecules can help to understand the magnetic ground state.

In X = Br, the effect of V is weaker than other salts with octahedral anions as mentioned above. In addition, this salt is 2D even at high temperature [Fig. 5(c)]. From these facts, it is reasonable to stabilize the AFM state in X = Br because of the theoretical prediction in Ref. [63].

The situation is more complicated for salts that cause the CO transition. There is not much difference in two-dimensionality among the CO phases of X = NbF_6, AsF_6, and PF_6 [Fig. 5(c)]. However, Yoshimi *et al.* pointed out that not only the two-dimensionality [63] but also the spin frustration (i.e., anisotropy of transfer integrals between the 1D-chain molecules) [64] affects the magnetic ground state in the CO phase. Therefore, we investigated the interchain transfer integrals (t_{b1} and t_{p1}).

Figure 5(f) shows the spin frustration factor $|t_{b1}|/|t_{p1}|$ in the interchain direction at 30 K. Although all salts that cause the CO transition have large values of $|t_{b1}|/|t_{p1}|(= 6$–$17)$ at 200 K (DMI phase) (Table S9 in the Supplemental Material [73]), the values approach 1; that is, t_{b1} and t_{p1} antagonize

at 30 K (CO phase) [Fig. 5(f)]. At 30 K, $|t_{b1}|/|t_{p1}| > 1$ in $X = PF_6$ and AsF_6, which show the SP order, but $|t_{b1}|/|t_{p1}| < 1$ in $X = NbF_6$, which shows the AFM order. This result is consistent with the previous theoretical prediction [64], in which the large t_{p1} contribution stabilizes the AFM state in the CO phase. In other words, because the salts with different magnetic ground states have different $|t_{b1}|/|t_{p1}|$ characters, the spin frustration may be a key parameter for understanding the SP and AFM states.

IV. SUMMARY

We have investigated the precise crystal structures of $(TMTTF)_2X$ using synchrotron XRD experiments. The $X =$ Br salt has a simple quasi-1D structure, but forms a relatively stronger 2D electronic state than other salts. In the $(TMTTF)_2X$ system with octahedral anions, the structural parameters are anisotropically variable with temperature because of the effect of steric hindrance of the octahedron. In these salts, since some quantum parameters antagonize, various electronic phases are realized on the *P-T* phase diagram. Our study provides important information for discussing complex interactions in a simple system.

ACKNOWLEDGMENTS

We thank Y. Nakamura and K. Sugimoto for supporting synchrotron XRD experiments, and K. Yoshimi, T. Tsumuraya, and H. Seo for fruitful discussions. This work was supported by a Grant-in-Aid for Scientific Research (Grant No. JP19J11697) from JSPS. The synchrotron radiation experiments were performed at SPring-8 with the approval of the Japan Synchrotron Radiation Research Institute (JASRI) (Proposals No. 2019A0070, No. 2019B0070, and No. 2020A0070). The ESR measurement was supported by Nanotechnology Platform Program (Molecule and Material Synthesis, Project No. JPMXP09S20MS1044) of the MEXT, Japan. The crystal structure and electron density distribution figures were visualized using VESTA [78].

[1] D. Jérome, A. Mazaud, M. Ribault, and K. Bechgaard, J. Phys. Lett. **41**, 95 (1980).
[2] D. Jérome and H. J. Schulz, Adv. Phys. **31**, 299 (1982).
[3] K. Kanoda, Hyperfine Interact. **104**, 235 (1997).
[4] H. Mori, S. Tanaka, and T. Mori, Phys. Rev B **57**, 12023 (1998).
[5] D. Jérome, Chem. Rev. **104**, 5565 (2004).
[6] M. Dressel, Naturwissenschaften **94**, 527 (2007).
[7] K. Kanoda and R. Kato, Annu. Rev. Condens. Matter Phys. **2**, 167 (2011).
[8] H. Kino and H. Fukuyama, J. Phys. Soc. Jpn. **65**, 2158 (1996).
[9] H. Seo, C. Hotta, and H. Fukuyama, Chem. Rev. **104**, 5005 (2004).
[10] H. Seo, J. Merino, H. Yoshioka, and M. Ogata, J. Phys. Soc. Jpn. **75**, 051009 (2006).
[11] H. Yoshioka, Y. Otsuka, and H. Seo, Crystals **2**, 996 (2012).
[12] J. L. Galigne, B. Liautard, S. Peytavin, G. Brun, J. M. Fabre, E. Torreills, and L. Giral, Acta Crystallogr., Sect. B **34**, 620 (1978).
[13] C. Coulon, P. Delhaes, S. Flandrois, R. Lagnier, E. Bonjour, and J. M. Fabre, J. Phys. (Paris) **43**, 1059 (1982).
[14] C. Coulon, S. S. P. Parkin, and R. Laversanne, Phys. Rev. B **31**, 3583 (1985).
[15] B. Köhler, E. Rose, M. Dumm, G. Untereiner, and M. Dressel, Phys. Rev. B **84**, 035124 (2011).
[16] B. Salameh, S. Yasin, M. Dumm, G. Untereiner, L. Montgomery, and M. Dressel, Phys. Rev. B **83**, 205126 (2011).
[17] F. Nad, P. Monceau, and J. M. Fabre, Eur. Phys. J. B **3**, 301 (1998).
[18] F. Nad, P. Monceau, C. Carcel, and J. M. Fabre, Phys. Rev. B **62**, 1753 (2000).
[19] F. Nad, P. Monceau, C. Carcel, and J. M. Fabre, J. Phys.: Condens. Matter **12**, L435 (2000).
[20] P. Monceau, F. Y. Nad, and S. Brazovskii, Phys. Rev. Lett. **86**, 4080 (2001).
[21] C. S. Jacobsen, D. B. Tanner, and K. Bechgaard, Phys. Rev. B **28**, 7019 (1983).
[22] M. Dressel, M. Dumm, T. Knoblauch, and M. Masino, Crystals **2**, 528 (2012).
[23] R. Swietlik, B. Barszcz, A. Pustogow, and M. Dressel, Phys. Rev. B **95**, 085205 (2017).
[24] M. Dumm, A. Loidl, B. W. Fravel, K. P. Starkey, L. K. Montgomery, and M. Dressel, Phys. Rev. B **61**, 511 (2000).
[25] M. Dumm, A. Loidl, B. Alavi, K. P. Starkey, L. K. Montgomery, and M. Dressel, Phys. Rev. B **62**, 6512 (2000).
[26] D. S. Chow, F. Zamborszky, B. Alavi, D. J. Tantillo, A. Baur, C. A. Merlic, and S. E. Brown, Phys. Rev. Lett. **85**, 1698 (2000).
[27] F. Zamborszky, W. Yu, W. Raas, S. E. Brown, B. Alavi, C. A. Merlic, and A. Baur, Phys. Rev. B **66**, 081103(R) (2002).
[28] T. Nakamura, J. Phys. Soc. Jpn. **72**, 213 (2003).
[29] W. Yu, F. Zhang, F. Zamborszky, B. Alavi, A. Baur, C. A. Merlic, and S. E. Brown, Phys. Rev. B **70**, 121101(R) (2004).
[30] S. Fujiyama and T. Nakamura, J. Phys. Soc. Jpn. **75**, 014705 (2006).
[31] T. Nakamura, K. Furukawa, and T. Hara, J. Phys. Soc. Jpn. **76**, 064715 (2007).
[32] F. Iwase, K. Sugiura, K. Furukawa, and T. Nakamura, J. Phys. Soc. Jpn. **78**, 104717 (2009).
[33] S. Hirose, A. Kawamoto, N. Matsunaga, K. Nomura, K. Yamamoto, and K. Yakushi, Phys. Rev. B **81**, 205107 (2010).
[34] F. Iwase, K. Sugiura, K. Furukawa, and T. Nakamura, Phys. Rev. B **84**, 115140 (2011).
[35] K. Furukawa, K. Sugiura, F. Iwase, and T. Nakamura, Phys. Rev. B **83**, 184419 (2011).
[36] S. Yasin, B. Salameh, E. Rose, M. Dumm, H.-A. Krug von Nidda, A. Loidl, M. Ozerov, G. Untereiner, L. Montgomery, and M. Dressel, Phys. Rev. B **85**, 144428 (2012).
[37] N. Matsunaga, S. Hirose, N. Shimohara, T. Satoh, T. Isome, M. Yamomoto, Y. Liu, A. Kawamoto, and K. Nomura, Phys. Rev. B **87**, 144415 (2013).
[38] S. Hirose, Y. Liu, and A. Kawamoto, Phys. Rev. B **88**, 125121 (2013).
[39] M. Asada and T. Nakamura, Phys. Rev. B **96**, 125120 (2017).

[40] L. N. Majer, B. Miksch, G. G. Lesseux, G. Untereiner, and N. Dressel, Appl. Magn. Res. **51**, 1321 (2020).
[41] J.-P. Pouget, R. Moret, R. Comes, K. Bechgaard, J. M. Fabre, and L. Giral, Mol. Cryst. Liq. Cryst. **79**, 485 (1982).
[42] S. Flandrois, C. Coulon, P. Delhaes, D. Chasseau, C. Hauw, J. Gaultter, J. M. Fabre, and L. Giral, Mol. Cryst. Liq. Cryst. **79**, 663 (1982).
[43] R. Laversanne, C. Coulon, B. Gallois, J.-P. Pouget, and R. Moret, J. Phys. (Paris) Lett. **45**, 393 (1984).
[44] L. Ducasse, M. Abderrabba, J. Hoarau, M. Pesquer, B. Gallois, and J. Gaultier, J. Phys. C: Solid State Phys. **19**, 3805 (1986).
[45] J.-P. Pouget and S. Ravy, Synth. Met. **85**, 1523 (1997).
[46] P. Foury-Leylekian, D. LeBolloch, B. Hennion, S. Ravy, A. Moradpour, and J.-P. Pouget, Phys. Rev. B **70**, 180405(R) (2004).
[47] Y. Nogami, T. Ito, K. Yamamoto, N. Irie, S. Horita, T. Kambe, N. Nagao, K. Oshima, N. Ikeda, and T. Nakamura, J. Phys. IV **131**, 39 (2005).
[48] P. Foury-Leylekian, S. Petit, G. Andre, A. Moradpour, and J.-P. Pouget, Phys. B (Amsterdam, Neth.) **405**, S95 (2010).
[49] E. Rose, C. Loose, J. Kortus, A. Pashkin, C. A. Kuntscher, S. G. Ebbinghaus, M. Hanfland, F. Lissner, T. Schleid, and D. Dressel, J. Phys.: Condens. Matter **25**, 014006 (2013).
[50] S. Kitou, T. Fujii, T. Kawamoto, N. Katayama, S. Maki, E. Nishibori, K. Sugimoto, M. Takata, T. Nakamura, and H. Sawa, Phys. Rev. Lett. **119**, 065701 (2017).
[51] J. P. Pouget, P. Foury-Leylekian, S. Petit, B. Hennion, C. Coulon, and C. Bourbonnais, Phys. Rev. B **96**, 035127 (2017).
[52] D. Jérome, Science **252**, 1509 (1991).
[53] J.-P. Pouget and S. Raby, J. Phys. I **6**, 1501 (1996).
[54] M. de Souza, P. Foury-Leylekian, A. Moradpour, J.-P. Pouget, and M. Lang, Phys. Rev. Lett. **101**, 216403 (2008).
[55] M. de Souza, D. Hofmann, P. Foury-Leylekian, A. Moradpour, J.-P. Pouget, and M. Lang, Phys. B (Amsterdam, Neth.) **405**, S92 (2010).
[56] M. de Souza and J.-P. Pouget, J. Phys.: Condens. Matter **25**, 343201 (2013).
[57] J.-P. Pouget, Crystals **2**, 466 (2012).
[58] E. Rose and M. Dressel, Phys. B (Amsterdam, Neth.) **407**, 1787 (2012).
[59] J.-P. Pouget, P. Alemany, and E. Canadell, Mater. Horiz. **5**, 590 (2018).
[60] H. Seo and H. Fukuyama, J. Phys. Soc. Jpn. **66**, 1249 (1997).
[61] S. Mazumdar, R. T. Clay, and D. K. Campbell, Phys. Rev. B **62**, 13400 (2000).
[62] Y. Shibata, S. Nishimoto, and Y. Ohta, Phys. Rev. B **64**, 235107 (2001).
[63] K. Yoshimi, H. Seo, S. Ishibashi, and S. E. Brown, Phys. Rev. Lett. **108**, 096402 (2012).
[64] K. Yoshimi, H. Seo, S. Ishibashi, and S. Brown, Phys. B (Amsterdam, Neth.) **407**, 1783 (2012).
[65] G. Giovannetti, S. Kumar, J.-P. Pouget, and M. Capone, Phys. Rev. B **85**, 205146 (2012).
[66] A. C. Jacko, H. Feldner, E. Rose, F. Lissner, M. Dressel, R. Valentí, and H. O. Jeschke, Phys. Rev. B **87**, 155139 (2013).
[67] G. Giovannetti, R. Nourafkan, G. Kotliar, and M. Capone, Phys. Rev. B **91**, 125130 (2015).
[68] K. Sugimoto, H. Ohsumi, S. Aoyagi, E. Nishibori, C. Moriyoshi, Y. Kuroiwa, H. Sawa, and M. Takata, in *The 10th International Conference on Synchrotron Radiation Instrumentation*, AIP Conf. Proc. No. 1234 (AIP, Melville, NY, 2010), p. 887.
[69] R. H. Blessing, Crystallogr. Rev. **1**, 3 (1987).
[70] V. Petříček, M. Dušek, and L. Palatinus, Z. Kristallogr. - Cryst. Mater. **229**, 345 (2014).
[71] T. Mori, A. Kobayashi, Y. Sasaki, H. Kobayashi, G. Saito, and H. Inokuchi, Bull. Chem. Soc. Jpn. **57**, 627 (1984).
[72] S. Kitou, T. Manjo, N. Katayama, T. Shishidou, T. H. Arima, Y. Taguchi, Y. Tokura, T. Nakamura, T. Yokoyama, K. Sugimoto, and H. Sawa, Phys. Rev. Research **2**, 033503 (2020).
[73] See Supplemental Material at http://link.aps.org/supplemental/10.1103/PhysRevB.103.184112 for the results of crystal structural analysis.
[74] R. D. Shannon, Acta Crystallogr. **32**, 751 (1976).
[75] T. C. Umland, S. Allie, T. Kuhimann, and P. Coppens, J. Phys. Chem. **92**, 6456 (1988).
[76] A. Volkov, P. Macchi, L. J. Farrugia, C. Gatti, P. Mallinson, T. Richter, and T. Koritsanszky, XD2016, a computer program package for multipole refinement, topological analysis of charge densities and evaluation of intermolecular energies from experimental or theoretical structure factors (2016).
[77] S. Kitou, Y. Hosogi, R. Kitaura, T. Naito, T. Nakamura, and H. Sawa, Crystals **10**, 998 (2020).
[78] K. Momma and F. Izumi, J. Appl. Crystallogr. **44**, 1272 (2011).